Astronomy & Astrophysics manuscript no. ms6444
April 16, 2007

Dust and Molecular Content of the Lensed Quasar, MG0751+2716, at $z = 3.2$

Danielle Alloin[1,2], Jean-Paul Kneib[3], Stéphane Guilloteau[4], and Michael Bremer[5]

[1] European Southern Observatory, Casilla 19001, Santiago 19, Chile
[2] AIM, CEA/DSM-CNRS-Université Paris 7, SAp, Bât.709, CE Saclay, l'Orme des Merisiers, 91191 Gif-sur-Yvette Cedex, France
[3] Laboratoire d'Astrophysique de Marseille, OAMP Traverse du Siphon, BP 8, 13376 Marseille Cedex 12, France
[4] Laboratoire d'Astrophysique de Bordeaux, CNRS, OASU, Université Bordeaux 1, BP 89, 33270 Floirac, France
[5] Institut de Radio Astronomie Millimétrique, 300 rue de la Piscine, 38406, Saint Martin d'Hères, France

Received ; Accepted

ABSTRACT

Context. Gravitational lenses offer unique opportunities to explore the molecular content around active galactic nuclei at high redshift, through the magnification and gain in angular resolution.
Aims. We study here the molecular and dust content of the high redshift (z=3.2), gravitationally lensed quasar MG0751+2716.
Methods. We used the IRAM Plateau de Bure interferometer to measure the CO J=3-2, J=4-3 and J=8-7 rotation lines and continuum flux between 1.1 mm and 3 mm in MG0751+2716. We use HST data and constraints from the high resolution MERLIN map at 6.2 cm to build an improved model of the lens.
Results. The position agreement between the CO emission and the millimeter continuum suggests that dust and molecules are closely related. A 500 km s^{-1} velocity gradient is tentatively detected from the CO lines across the central $0.5''$. The continuum SED in the range 0.45 mm – 204 mm exhibits the signatures of two components: synchrotron emission from a core/jet system, and thermal emission related to warm dust. The CO line intensities are compatible with warm, dense molecular gas, suggesting a location in the close environment of the quasar. These observational constraints lead us to consider a source/quasar model made of a point-like core, a radio jet, and a molecular and dusty ring-like structure (∼460 pc in radius) located in a plane perpendicular to the jet axis and seen almost edge-on. For this configuration, we derive a total magnification of 16 for the quasar radiation at rest frequency above 350 GHz and a magnification of 25 below 350 GHz. The dust mass (assuming a likely temperature T=50 K) is $M_{dust} = 1.7 \times 10^8$ $M_\odot$, the mass of molecular material is $M(H_2) = 6 \times 10^{10}$ $M_\odot$ and a lower limit to the dynamical mass is $M_{dyn} = 1.5 \times 10^{10}$ $M_\odot$. Such values are comparable to those found in the small sample of CO detected sources at high redshifts.

Key words. gravitational lensing – quasar: high redshift – quasar: individual (MG0751+2716) – quasar: dust – quasar: molecules – cosmology: observations

1. Introduction

With the aim of tracing back the formation and evolution of galaxies, major efforts have been devoted over the past decade to the obtention of direct information about the dust and molecular content of the early Universe ($z \gtrsim 1.5$). The search for CO and HCN molecules in high redshift sources (including quasars, QSOs, ultra-luminous infrared galaxies -ULIRGs-, submillimeter galaxies -SMGs-, radio galaxies, etc) is part of this effort, engaging a number of millimeter dishes and arrays in the adventure. To date, a few tens of such sources have been detected, up to the very distant quasar SDSS J1148+5251 at redshift $z = 6.42$ (Fan et al. 2003; Walter et al. 2003): see compilations and reviews by Wiklind & Alloin (2002); Hainline et al. (2004); Greve et al. (2005); Carilli et al. (2005).

In the study of sources at redshift beyond 1.5, strong gravitational lensing, whenever at work, provides the following advantages for unresolved sources: (a) thanks to amplification factors up to a few tens, a gain in flux which is critical in the detection of distant and faint objects, and (b) in the case of favorable geometry, a spectacular gain in spatial resolution. Indeed, for a source made of subcomponents with different positions on the sky, the comparison of lensed images at various wavelengths (each wavelength being selected as characteristic of roughly one physical sub-component within the source) provides a unique opportunity to isolate and separate the sub-components within the source, that is to explore its structure and geometry (e.g. Narayan & Wallington 1993). One of the first applications of this tool for probing the structure of a high redshift QSO was the analysis of the Cloverleaf, a BAL QSO at $z = 2.58$ (Kneib et al. 1998). More recently, Krips

Send offprint requests to: D. Alloin, e-mail: danielle.alloin@cea.fr

[1] Based on observations carried out with the IRAM Plateau de Bure Interferometer. IRAM is supported by INSU/CNRS (France), MPG (Germany) and IGN (Spain). Based on observations obtained with the NASA/ESA Hubble Space Telescope, obtained from the data archive at the Space Telescope Science Institute. STScI is operated by the Association of Universities for Research in Astronomy, Inc. under the NASA contract NAS 5-26555.

et al. (2005) applied a similar treatment in the study of the doubly lensed quasar Q0957+561. Given the promises of this technique and with the perspective of future studies with ALMA, we completed a CO survey of gravitationally lensed quasars with the IRAM Plateau de Bure interferometer (PdBI), in the course of which the source MG0751+2716 at $z = 3.2$ was discovered to be a strong CO emitter (Barvainis et al. 2002).

The lensed nature of the quasar MG0751+2716 (Lawrence et al. 1986) was unveiled by VLA observations at 2.0 cm, 3.6 cm and 6.2 cm (Lehar et al. 1997), showing four images, A through D, of the radio quasar, with the A, B and C images joining in an arc-like feature. The maximum separation between images is $0\farcs9$. In addition, the MERLIN array was used to provide higher spatial resolution: each of the A, B and C images then became resolved in a set of sub-images, such as A1, A2, A3..., revealing the presence of sub-components within the radio source. A first model of the lens was proposed by Lehar et al. (1997). It included a galaxy (G3) as the principal lensing galaxy, while the gravitational impact of other nearby galaxies, likely forming a galaxy group, was taken into account in different ways: either as individual galaxies, or by including a group scale mass distribution (see Section 3 of this paper). Their final model allowed to associate the sub-images observed with the MERLIN array with the following sub-components in the source: a radio core (S1) and a radio jet along which a series of knots were identified (S2 close to the core, S3-S4, S5 and possibly S6).

Spectroscopic redshifts of galaxies in the field around MG0751+2716 have later been obtained with KeckII (Tonry & Kochanek 1999), confirming that G3 belongs to a group of galaxies at $z = 0.350$ and providing the precise redshift of the source, $z = 3.200$.

At the time of its discovery as a CO line emitter (Barvainis et al. 2002), the J=4-3 transition was measured and an upper limit on J=9-8 was derived; moreover, continuum flux densities were obtained at 2.7mm and 1.2mm. Later, HCN line emission from this source was searched for, with the VLA, by Carilli et al. (2005). Only an upper limit was derived for the HCN line, while a partially resolved continuum map was obtained at 42.2 GHz.

In this paper, we present new millimeter observations of MG0751+2716 including the CO J=3-2, J=4-3 and J=8-7 lines and continuum points at 1.4, 2.7 and 3.6 mm (Section 2). Taking advantage of the more precise constraints brought by the HST dataset, we propose a new model of the lens in Section 3, and finally we discuss the dust and molecular content of MG0751+2716 in Section 4. Throughout we use $H_0 = 70\,\mathrm{km\ s^{-1}/Mpc}$, $\Omega_m = 0.3$ and $\Omega_\lambda = 0.7$. At redshift $z = 3.200$ the scale factor is thus 7.5 kpc/″.

2. New Millimeter observations of MG0751+2716

Following the discovery of MG0751+2716 as a high redshift CO emitter (Barvainis et al. 2002), new observations were collected using the six antennas of the IRAM PdBI, on 2002 January 8 (3.6 mm and 1.4 mm) and on 2003 March 5 and 7 (2.7 mm and 1.4 mm), offering a maximum baseline of 368 m. Observations were performed under good weather conditions with low precipitable water content and seeing from $0\farcs26$ to $0\farcs69$ (as derived from phase noise). Two quasars 0738+313 and 0827+243 were used

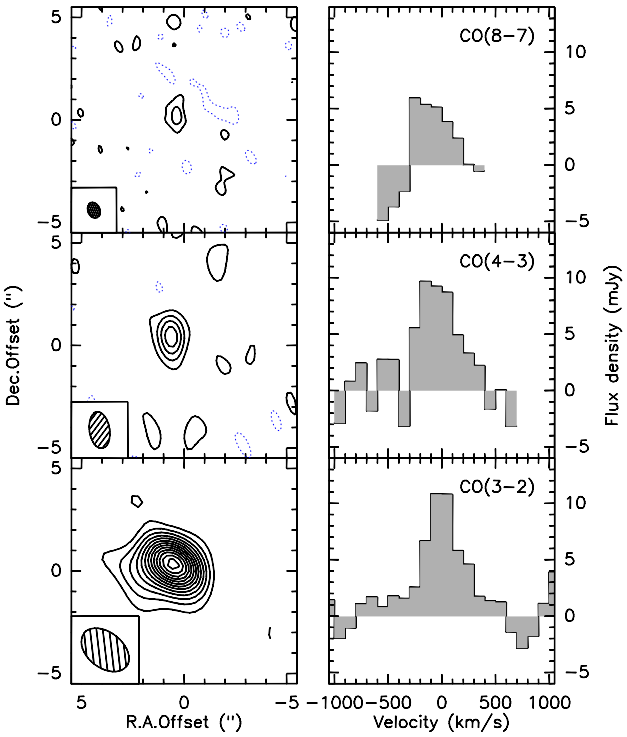

Fig. 1. CO maps and velocity line profiles of MG0751+2716 for the 3 transitions J=8-7, J=4-3 and J=3-2 [from top to bottom]. For each CO transition, the left panel shows the map, with reference coordinates $\alpha_{J2000} = 07^{\mathrm{h}}51^{\mathrm{m}}41\fs460$ and $\delta_{J2000} = 27°16'31\farcs40$ and with an insert providing the beam shape, size and orientation, while the right panel shows the line profile, referred to a redshift of 3.200. First contour and contour steps are 0.6 Jy km $\mathrm{s^{-1}}$/beam ($\approx 2\sigma$) for the J=8-7 line, and 0.3 Jy km $\mathrm{s^{-1}}$/beam ($\approx 2\sigma$) for the J=4-3 and 3-2 lines.

respectively as phase calibrator and flux calibrator. The coordinates for the pointing reference of the PdBI were: $\alpha_{J2000} = 07^{\mathrm{h}}51^{\mathrm{m}}41\fs460$ and $\delta_{J2000} = 27°16'31\farcs40$. System temperatures were in the range 110 to 170 K at 3.6 mm, 140 to 200 K at 2.7 mm and 200 to 400 K at 1.4 mm.

The data reduction was performed using the IRAM PdBI pipeline and the final data were scaled to a source redshift $z = 3.200$. The source is well detected in the CO J=3-2, J=4-3 and J=8-7 transitions (Fig. 1), as well as in their neighboring millimeter continuum. Although the CO J=9-8 line is not included in this dataset, we recall here the values found in Barvainis et al. (2002), in particular the CO J=9-8 line intensity upper limit of 2 Jy km $\mathrm{s^{-1}}$ and a continuum detection at 1.3mm of 6.7±1.3 mJy (see Table 5).

2.1. Continuum

The source is partially resolved by the interferometer, in the sense that the visibilities exhibit a significant decrease with baseline length, but the angular resolution is not sufficient to fully separate the quasar images (see Table 1). Accordingly, to avoid the beam-size dependent bias on the total flux which would result from a point source approximation, we have estimated the flux densities by using two priors for the source structure. We fitted an annular shape with a radius of $0\farcs45$, a width of $0\farcs15$, i.e. a prior matching very closely the quasar image at centimeter wavelengths.

Table 1. Continuum emission of MG0751+2617, from 1mm to 3mm.

Frequency		Beam size	PA	RA	DEC	Flux
Observed (GHz)	Rest (GHz)	(″× ″)	(°)	(J2000)		(mJy/beam)
82.372	345.962	2.7 × 1.7	+52	07:51:41.500	27:16:31.68	5.1±0.4
109.824	461.261	1.8 × 1.0	+7	07:51:41.475	27:16:31.54	3.0±0.5
219.581	922.240	0.9 × 0.7	+62	07:51:41.494	27:16:31.49	4.3±0.8

Table 2. Parameters of the CO line profiles (reference at $z = 3.200$) and line fluxes as measured after spatial fitting of a circular Gaussian with a FWHM of 0.7”

CO transition	FWHM (km/s)	Gaussian center (km/s)	Flux (Jy.km/s)
J=3-2	400 ± 50	5 ± 20	4.6 ± 0.5
J=4-3	390 ± 70	-35 ± 30	4.2 ± 0.7
J=8-7	400 (fixed)	-15 (fixed)	2.2 ± 0.7

Using a simpler prior, a circular Gaussian with a FWHM of 0.″7 gives essentially the same results (but a 1″ Gaussian would overestimate flux densities by 10 to 20%). Therefore, in the following we have performed all our measurements using a circular Gaussian with a FWHM of 0.″7. The resulting millimeter continuum flux densities are displayed in Table 1.

We have tentatively compared the absolute position of the surface brightness peak derived from the PdBI dataset to those derived from other radio datasets, namely the 6 mm VLA (Carilli et al. 2005) and the 6.2 cm MERLIN (Lehar et al. 1997) datasets. Because of the very different angular resolution, the comparison is not straightforward, despite the 0.″05 astrometric accuracy. We have used instead the best isolated - hence best defined - image D of the quasar to first register the MERLIN map with respect to the 6 mm VLA map. Then through comparisons with the 6 mm VLA map, we have found that the PdBI millimeter surface brightness peak falls in between the three 6 mm VLA surface brightness peaks, and slightly closer to image A, which is the strongest at 6 mm. This is illustrated on Fig. 2. Such a result is consistent with the fact that the PdBI beams are larger than the VLA beam (0.″4). It also suggests that image A is the brightest on all millimeter maps from 6 mm down to 1 mm. Comparison of the 6 mm VLA map with the MERLIN high resolution map at 6.2 cm additionally indicates that the quasar subimages which contribute most to the emission at 6 mm (hence likely all through the millimeter range, as suggested above) are A1 and A2, corresponding to sub-components S1 (core) and S2 (the jet-knot closest to the core). The other sub-components S3 through S6 display prominent images mostly at centimeter wavelengths and are likely related to a jet emission which is fading away at shorter wavelengths.

2.2. CO line measurements

As for the continuum, the lines have been extracted after spatial fitting of a circular Gaussian with FWHM of 0.″7 to include all the flux. We subtracted the underlying continuum. For the CO J=8-7 line, the instrumental bandwidth of the signal sideband was insufficient to determine the continuum (Fig. 1, upper right graph), which was instead accurately determined from the image sideband of the (DSB) receivers, 3 GHz away from the line. Fig. 1 shows the resulting images and line profiles: the three transitions J=3-2, J=4-3 and J=8-7 of CO have been detected with excellent (> 25) to fair (~ 6) signal to noise ratios.

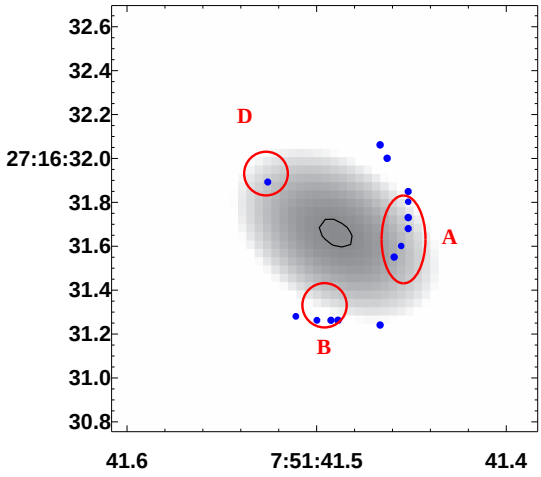

Fig. 2. Relative position of the different radio dataset. Small (blue) points are the MERLIN positions of the various subcomponent, large ellipses (red) are the positions of the VLA map which has been shifted in alpha to match the MERLIN position. The grey image is the continuum map at 3mm with a thin black ellipse giving the relative uncertainty in the center position.

At the achieved signal to noise ratios, the three lines display symmetrical profiles. In a subsequent step, the line profiles have been fitted in velocity space with a single Gaussian, for which the central position, the FWHM and the amplitude were set free (except the CO J=8-7 line for which the FWHM and center have been fixed because of the limited signal to noise ratio). The results are given in Table 2.

Considered altogether, the J=4-3 and J=3-2 transitions exhibit a mean peak of emission at -20 km s^{-1} with respect to the reference $z = 3.2000$, which gives a precise CO emission redshift of $z = 3.1999$. Their FWHM, around 400 km s^{-1}, is similar to those observed in a sample of high redshift CO-detected QSOs (see the compilation in Hainline et al. 2004). Compared to the discovery observation by Barvainis et al. (2002), this new measurement of the CO J=4-3 transition is in excellent agreement with regard to the line FWHM and within about 2σ with regard to the line flux, which, given the uncertainties associated with the measure of such faint lines in the millimeter domain, is acceptable.

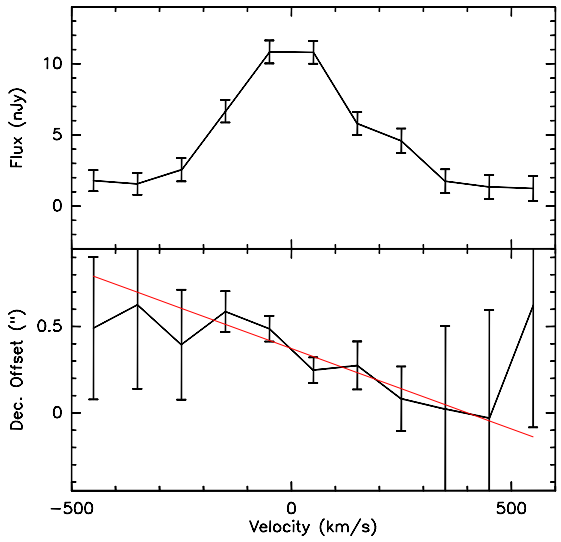

Fig. 3. Top: CO J=3-2 line profile at 100 km s^{-1} spectral resolution. Bottom: Declination offset as function of velocity for the CO J=3-2 line. Error bars are $\pm 1\sigma$. The straight line is the best fit of a constant velocity gradient, ΔV of 540 km s^{-1} over 0.5″.

Table 3. Positional offsets in the PdBI continuum and CO lines, with respect to the PdBI positional reference given in Section 2: J2000, RA = 07:51:41.460, DEC = 27:16:31.40.

Frequency/Line (GHz)	$\Delta\alpha$ (arcsec)	$\Delta\delta$ (arcsec)
82	0.50 ± 0.06	0.22 ± 0.06
CO J=3-2	0.56 ± 0.06	0.28 ± 0.06
110	0.20 ± 0.10	0.15 ± 0.15
CO J=4-3	0.54 ± 0.10	0.36 ± 0.15
220	0.45 ± 0.08	0.10 ± 0.08
CO J=8-7	0.45 ± 0.08	0.10 ± 0.08

For the J=3-2 transition, a velocity gradient appears as a function of declination, with velocity difference of $\approx$ 500 km s^{-1} across the 0.″5 central region, and with a significance level of 3.9σ (see Fig. 3). We did check whether such a gradient is also present in the other two transitions CO J=4-3 and J=8-7, which, however, are of much lower signal to noise ratio. Using a weighted combination of the three lines, the significance of the gradient is lowered to 3σ. Obviously this result needs further confirmation; yet, we examine in Section 4 its potential implication on the structure of the source.

Additionally, it is interesting to find out where the millimeter continuum emitting dust is located with respect to the CO line emitting molecular gas. This can be achieved by comparing the relative positioning of the surface brightness peaks in the PdBI millimeter continuum maps and CO transition maps. Table 3 provides these measured relative positional offsets. The set of 12 measurements looks fairly homogeneous, with one value at 3σ (RA position of the 110 GHz continuum) which is to be expected on the grounds of pure statistics. Therefore, we conclude that, altogether, there is no significant offset among the 6 line and continuum surface brightness peaks. This indicates that the warm dust thought to be responsible for the millimeter continuum is located close to the molecular component.

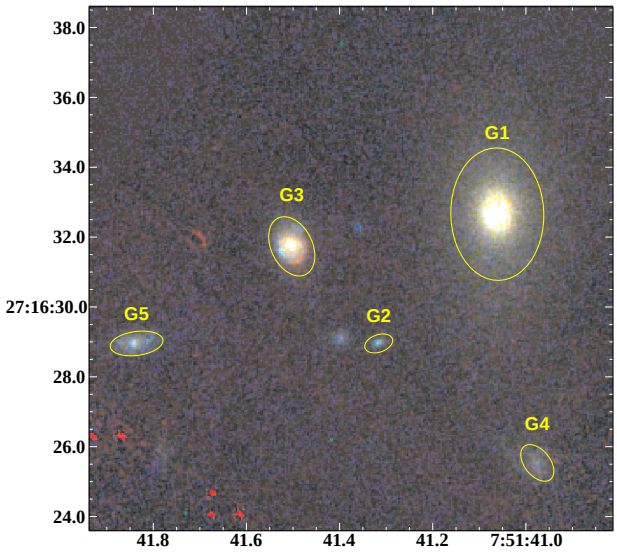

Fig. 4. Hubble WFPC2 (F555W and F814W) and NICMOS (F160W) color image of the MG0751+2716 system where we have identified the different galaxies used in the lens modeling. The relative size of the ellipse is proportional to the mass contribution of each galaxy

The interpretation of these new measurements in terms of the intrinsic properties of the molecular gas in the quasar requires that we first obtain a good model of the lens, so that the amplification factor can be derived safely and applied to the observed quantities, whenever relevant.

3. A revised model of the lens towards MG0751+2716

Since the early lens model by Lehar et al. (1997), additional information on this system has been collected. A set of HST observations with the filters F555W, F814W of the WFPC2 camera and with the filter F160W of the NICMOS camera has become publicly available in the archive. Moreover, the measurement of spectroscopic redshifts of galaxies in the field (Tonry & Kochanek 1999), has confirmed the presence of a galaxy group at $z = 0.3501$, to which the principal lensing galaxy at $z = 0.3502$ belongs. Such new elements allow building an improved model of this lens.

We have retrieved and reduced with standard packages the HST dataset, in order to derive more precise parameters for the group galaxies, such as their center position and luminosity profile whenever accessible (we follow the galaxy identifications given by Lehar et al. 1997). Our improved model of the lens takes into account the galaxies G3 (the main lensing galaxy), G1, G2, G4, G5 (each with its dark matter halo), plus a global dark matter halo associated with the dark matter component of the group. Note however that the dominant contributors to the multiple image system of the quasar are G3, G1 and the dark matter halo (Fig. 4). The positions of the galaxies G1-5 were measured using SExtractor (Bertin & Arnouts 1996) on the WFPC2/F814W data, and are given relative to the main galaxy G3 in Table 3. Compared to the positions given in Lehar et al. (1997) there is a fair agreement (considering the much lower image resolution of the previous optical data used by Lehar et al. (1997)), except for the fainter

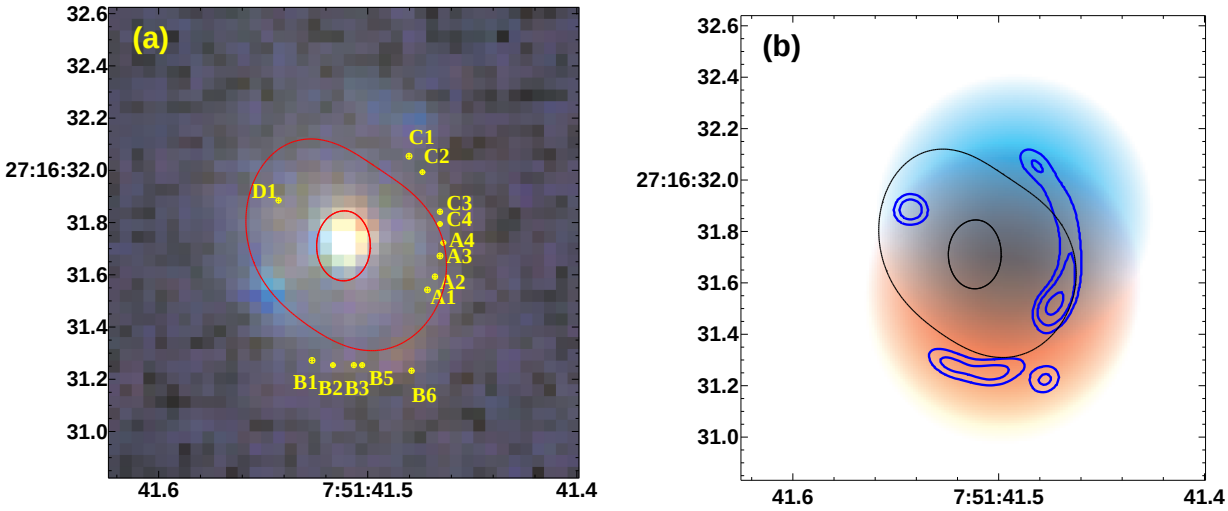

Fig. 6. (a) The image plane: identified radio components (numbered capital letter A1, A2, A3.... through D1) by Lehar et al. (1997) superimposed on the color HST (WFPC2/NICMOS) image of G3. The curves show the critical lines. (b) The image plane: images of the core and jet (green contours), and color image of the dust/molecular ring convolved by a 2″ circular beam to match the mean beam of the PdBI millimeter dataset. The velocity gradient in declination, is illustrated through the color evolution across the image of the dust/molecular ring emission.

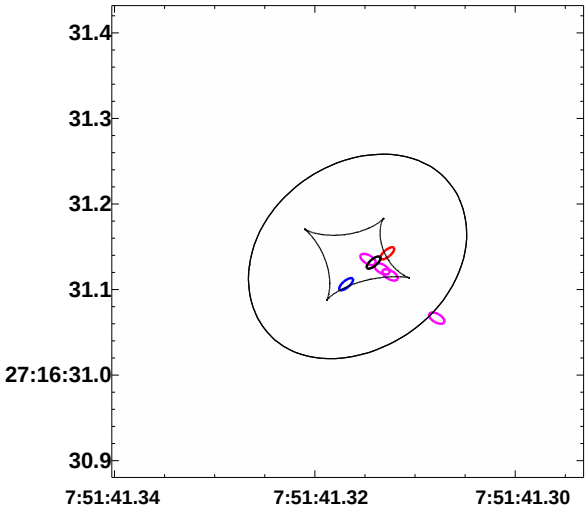

Fig. 5. The source plane: caustic lines, model for the core and knotted jet (magenta ellipses) and model for the dust/molecular ring (blue/black/red ellipses) with radius 0.″06 (translating into an intrinsic radius of ∼460 pc with the chosen cosmology) and orientation with respect to the radio jet, chosen in order to reproduce the velocity gradient along declination observed in the CO J=3-2 transition. The slight offset in coordinates between the source and the image planes (see Fig.6) results from the lensing shear of the galaxy group.

galaxy G2 which has been resolved by HST in two different galaxies. We only retained the brighter one in our analysis.

We used the LENSTOOL software (http://www.oamp.fr/cosmology/lenstool/) to model MG0751+2716, as this software can easily handle a large number of mass components. Each mass component was modeled by a truncated pseudo isothermal elliptical mass distribution (PIEMD, see for example Kneib et al. (1996)), which has a flexible behavior and can easily mimic galaxy mass profiles (for a vanishing core) or more extended mass profiles such as group or cluster mass profiles. The lens model is essentially constrained in the image plane by the positions of the different images identified on the radio 6.2 cm MERLIN map. Because of the likely time variability of the radio source, hence of the radio images, and the difficulty in separating the different radio sub-components, we did not fit the radio fluxes.

Faint optical features can be seen around G3 in the HST image. Although, in principle, they could be used as additional constraints for the modeling, we chose not to take them into account as we are uncertain of their redshift and of their real association with the lensed source. The best model parameters are displayed in Table 4. Using this model, the reconstructed source plane and image plane are shown respectively in Fig. 5 and Fig. 6. In Fig. 5, we display in the source plane, the caustics of the lens model and the various sub-components we have considered in the source. Similarly to Lehar et al. (1997), the centimeter radio emission is modeled with a core (S1) and nearby sub-component S2, as well as a knotted jet (sources S3 to S5). In order to match the characteristics of the new millimeter observations, and particularly the velocity gradient tentatively observed in declination across the CO J=3-2 line map, we have added an edge-on molecular ring/disk. By adjusting its position and size, we find this ring to be roughly orthogonal to the projection on the sky of the radio jet, and to have an extension of about 0.″06 (corresponding to an intrinsic radius of ∼460 pc, since with the adopted cosmology, 1″ corresponds to 7.55 kpc at $z = 3.2$). In the panel (a) of Fig. 6, we show overlaid on the composite (F555W, F814W, F160W) Hubble image, the critical lines of our lens model, together with the observed centimeter radio positions. The predicted image in the CO line emission of the dust/molecular ring convolved by a 2″ circular beam to match the mean beam of PdBI is shown on panel (b) of Fig. 6. The color gradient represents the velocity gradient tentatively observed in the CO(3-2) line. The new generation of millimeter interferometers should allow to check our predictions: improvement in spatial resolution and sensitiv-

ity will provide separate images in the CO line blue-wing and the CO red-wing, hence a direct probe of the velocity-position gradient.

The model predicts amplification factors which vary according to the image considered (A through D) and to the sub-component considered within the source as a result of its location with respect to the inner caustic line of the model. The latter dependence may introduce some chromatic effects. Therefore, one should be cautious in the derivation of the total magnification (all images A through D included) and fully understand the chromatic effects resulting from the source structure. In MG0751+2716, the component within the source which dominates the continuum emission shortwards of 2 mm and is also responsible for the CO line emission (the dust/molecular ring), is subject to a total magnification of about 16. For the continuum emission at wavelengths longer than 2 mm, the magnification depends on the sub-component considered (core versus jet): our lens model predicts a total amplification factor of 25 for the sub-components S1 to S5, while S6 is subject to a smaller amplification factor of 11. This sub-component is however negligible in terms of its contribution to the total radio flux and we retain an amplification factor of 25 for the continuum points longwards of 2 mm.

4. The dust and molecular content of MG0751+2716

The spatial resolutions achieved in the PdBI dataset are not high enough to fully resolve the four images of the quasar emission at millimeter wavelengths and only a tentative velocity gradient has been measured from the CO J=3-2 transition. Yet, some quantities can be derived, at first order, regarding the dust and molecular content of the quasar MG0751+2716.

4.1. The continuum spectral energy distribution (SED) of MG0751+2716: dust mass

From the compilation of the flux densities (Table 5) measured for MG0751+2716 in the range of observed frequencies 660 to 1.47 GHz we show on Fig. 7(a) the observed continuum SED of MG0751+2716. At first glance, the presence of two distinct contributions is suggested:

- synchrotron emission in the range 20.4 cm to 3 mm with a slope of -1.35 and a signature of self-absorption at 20.4 cm which is typical of radio cores and radio jets,
- the pronounced dip between 2 mm and 1 mm, followed by a steep rise from 1 mm to 0.85 mm is reminiscent of thermal emission from warm dust heated by the quasar central engine.

The leveling off at 0.45 mm is similar to that observed in other high redshift quasars, e.g. on the SED of the Cloverleaf at $z = 2.58$ (Weiß et al. 2003). The intrinsic SED has been derived according to the adopted cosmological parameters, and is displayed in the quasar rest-frame in Fig. 7 (b). Two different values of the magnification factor have been used to derive the absolute quasar luminosity following the discussion in Section 3: *i)* 16 for points at rest frequencies above 350 GHz; *ii)* and 25 for points at rest frequencies below. Note that these new magnification figures remain close to the mean value quoted in Barvainis et al. (2002) following a private communication by Lehar and McLeod.

The leveling off in luminosity at 0.45 mm seen on Fig. 7 (b) suggests the contribution of dust at intermediate temperatures (40–50 K or slightly above). Unfortunately no data points are available in the far infrared and the fall off of the thermal dust emission at higher frequencies is not observed, which prevents to derive a more accurate value. Assuming that the source in MG0751+2716 is similar to the Cloverleaf (Weiß et al. 2003) we tentatively consider that the dominant contribution to the dust mass is from a component at T=50 K (in the Cloverleaf, there is a ratio around 100 between the 50 K dust mass and the 115 K dust mass). Taking into account the difference in magnification between the two quasars and their respective flux ratios at 0.85 mm, we obtain an approximate mass of dust in MG0751+2716, $M_{dust} = 1.7 \times 10^8$ $M_\odot$.

A more reliable estimation of the dust mass in this object will have to wait for data points at higher frequencies than available, e.g. Spitzer data.

4.2. Properties of the molecular gas

Three CO transitions have been detected and measured in MG0751+2716, J=3-2, J=4-3, J=8-7 (see Table 2) and an upper limit is provided for an additional transition, J=9-8 (2 Jy km s^{-1}). The small number of transitions available for this object does not allow a full analysis of the CO SED (flux density versus rotational quantum number) to be performed, and the molecular gas physical conditions to be derived, as in other cases ((Barvainis et al. 1997; Bayet et al. 2004; Weiß et al. 2005a,b)). Here, we propose a quick and tentative estimation, through comparison with a sample of objects likely to resemble MG0751+2716 (high redshift sources and/or molecular components in nearby galaxy centers). Such sources (SMMJ16359+6612, Br1202, NGC253 central gas, M82 high excitation central gas) have been discussed and fitted through LVG models by Weiß et al. (2005b). They indicate the presence of dense and warm molecular gas ($N(H_2)$ from 10^3 to 10^4 cm^{-3} and T_{kin} from 30 K to 50 K). The set of CO transitions detected in the different sources varies according to redshift and the flux densities are commensurate with distance: therefore it is more appropriate to discuss normalized figures over the full CO SED from J=1-0 to J=9-8. After Weiß et al. (2005b), and for the considered sample of sources, the flux ratio of the transitions J=3-2 to J=1-0 is around 8. Assuming that a similar ratio holds true for MG0751+2716 we obtain the following flux ratios with respect to J=1-0, successively for the transitions J=4-3, J=8-7 and J=9-8: 7.3±1 to 10.5±1(two values depending on the figure used for CO J=4-3, this paper or Barvainis et al. 2002), 3.8±1, and <3.5. The turnover of the CO line SED for MG0751+2716 occurs between the transitions J=4-3 and J=8-7 but cannot be located precisely: access to the CO J=6-5 and J=7-6 transitions are mandatory to model with accuracy the physical conditions of the molecular gas in MG0751+2716. Comparison with the objects discussed in Weiß et al. (2005b), tentatively suggests that the molecular gas in MG0751+2716 giving rise to CO transitions from J levels above 3, has physical conditions close to those encountered at the center of NGC253 or in SMMJ16359+6612: dense gas ($N(H_2) \sim 10^4$ cm^{-3}) and T_{kin} above 50 K.

Table 4. Fiducial model parameters for MG0751+2617. Bold numbers were fitted when modeling the lens systems, others were fixed using the galaxy position and shape information, and using standard scaling relation (such as the Faber-Jackson relation) for the mass profile. The mass profiles used are truncated pseudo isothermal elliptical mass distributions (PIEMD) see for example Kneib et al. (1996). The measurement accuracy of the galaxy positions G1-G5 in the HST/WFPC2 image is typically 0.02″

Component	$\Delta\alpha$, $\Delta\delta$ (", ")	ε, PA (-, deg)	σ (km/s)	Core Radius (")	Cut Radius (")
G3	0,0	**0.39,16**	**101**	0.05	**11**
DM Halo	**-5.6,-4.7**	0,0	**260**	4	100
G1	-5.88,0.92	0.34,1	240	0.05	24
G2	-2.49,-2.78	0.4,110	45	0.05	2
G4	-7.03,-6.20	0.4,40	80	0.05	2
G5	4.44,-2.78	0.6,98	60	0.05	2

Table 5. Observed SED of MG0751+2716

Wavelength (mm)	Observed freq. (GHz)	Rest freq. (GHz)	Observed flux density (mJy)	Ref.
0.45	660	2772	71 ±15	(1)
0.85	350	1470	25.8 ±2.6	(1)
1.2	246	1033	6.7 ±1.3	(2)
1.35	220	924	4.3 ±0.8	this work
2.7	110	462	3.0 ±0.5	this work
3.6	82	344	5.1 ±0.4	this work
7.1	42	176	13.2 ±0.1	(3)
20	15	63	48 ±4	(4)
36	8.3	35	104 ±1	(4)
62	4.8	20	191 ±1	(4)
204	1.5	6	413 ±1	(4)

(1) Barvainis & Ivison (2002), (2) Barvainis et al. (2002), (3) Carilli et al. (2005), (4) Lehar et al. (1997)

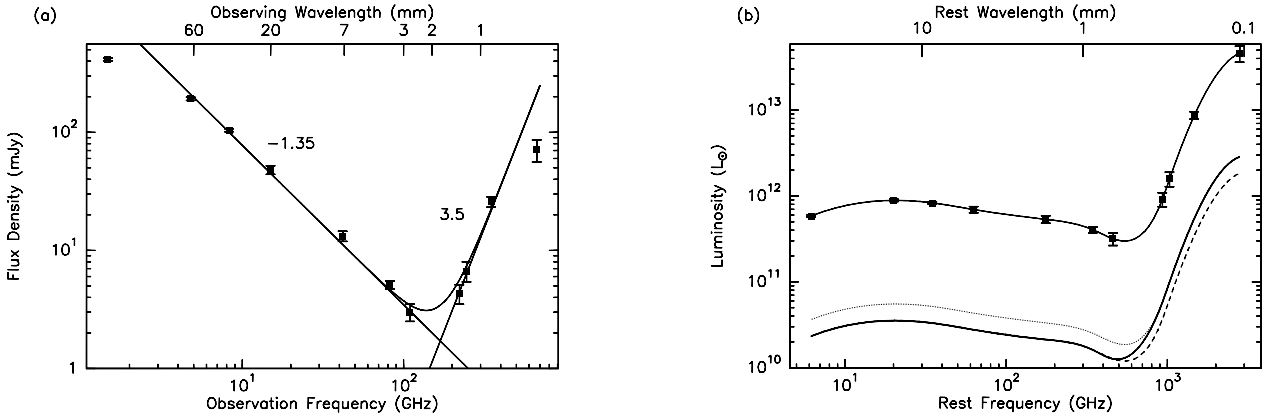

Fig. 7. (a): observed SED of MG0751+2716: data points, power law fits and exponents. (b): the top curve displays the apparent luminosity of MG0751+2716 (data point and fit). The bottom curves correspond to the intrinsic luminosity after corrections for the lens magnification (dotted line $m = 16$, dashed line $m = 25$, thick line: adopted differential magnification as discussed in Section 3).

From the velocity-integrated flux in the CO J=3-2 line, we can estimate the CO line luminosity, using the formulae in Solomon et al. (1992). We obtain: L(CO)= $2.9 \pm 0.3 \times 10^8 m^{-1}$ $L_\odot = 2.2 \pm 0.2 \times 10^{11} m^{-1}$ K. km s^{-1}.pc^2, where m is the magnification factor due to the lens.

Using a value of the transformation factor α between L(CO) and the total mass M(H_2), appropriate for the likely conditions of the gas in MG0751+2716 (warm and dense gas as in ULIRGs and around massive black holes), $\alpha = 4$ $M_\odot$ (K km $s^{-1}pc^{-2}$) from Solomon et al. (1997), we derive: $M(H_2) = 8.7 \times 10^{11} m^{-1}$ expressed in $M_\odot$. With a magnification of 16 (see Section 3), we obtain: $M(H_2) = 6 \times 10^{10}$ $M_\odot$.

Finally, we can derive the dynamical mass of the molecular component from the CO line profile and from the estimation of the size of the molecular disk/ring in the source deduced from the observed positional offset between the blue and red halves of the CO J=3-2 line and after applying the lens transformation,

$$M_{dyn} = \frac{r\delta V^2}{G \sin^2(i)}$$

where r is the radius of the molecular component, δV the FWHM of the CO line profile, G the constant of gravitation and i the inclination of the molecular disk/ring. Using the parameters derived in Section 3, r is around ∼460 pc and the disk/ring roughly edge-on. With a CO line FWHM of 400 km s^{-1}, we obtain $M_{dyn} = 1.5 \times 10^{10} \sin^{-2} i\ M_\odot$.

In conclusion, the characteristics we obtain for the molecular and dust components in MG0751+2716 can be summarized as follows (corrected for the lens magnification 16 and assuming a perfectly edge-on disk/ring, hence M_{dyn} is a lower limit):
$M_{dust} = 1.7 \times 10^8\ M_\odot$,
$M(H_2) = 6 \times 10^{10}\ M_\odot$,
$M_{dyn} = 1.5 \times 10^{10}\ M_\odot$.

The molecular mass exceeds the dynamical mass, although by a small factor. It would be easy to reconcile the two quantities. Either one could change the inclination of the molecular ring (30°). Or, this mismatch is a natural consequence of the molecular gas being located in the close environment of the quasar, the strong radiation field of which would support through radiation pressure the molecular gas against its self gravity. Such a situation is not uncommon in high redshift CO sources often associated with quasars or ULIRGs (Scoville et al. 1995).

Unfortunately, we have no access to the stellar mass in the kpc (diameter) central region around the massive black hole powering the radio quasar.

5. Discussion and concluding remarks

Regarding its content in molecular material, we find that MG0751+2716 is a system quite comparable to submillimeter-bright quasars also detected in CO at z between 2.56 and 2.86 (Kneib et al. 1998; Hainline et al. 2004, e.g.) or to HR10 at $z = 1.44$ (Andreani et al. 2000).

From the values derived in Section 4, we find that the intrinsic molecular gas mass and dust mass in MG0751+2716 are typical of those obtained for other high redshift galaxies (see e.g. Frayer et al. 1998) and that the gas to dust mass ratio is around 300, again a likely value in such objects.

A relevant question is whether the molecular/dust component observed in these objects is related to a molecular torus associated with the quasar activity or to the quasar host galaxy.

For a few lensed quasars with favorable geometry, differential gravitational effects allow to estimate the size of the CO-emitting source: in the Cloverleaf (Kneib et al. 1998; Venturini & Solomon 2003), in Q0957+561 (Krips et al. 2005) and in MG0751+2716. However, in this procedure, one also relies on a lens model which induces some uncertainty, for example in the Cloverleaf a factor 3 on the source size. In spite of this limitation, in the objects where thermal (T ≈ 50 K) dust emission is also detected, the radius of the CO-emitting source is found in the range 250 pc to 1 kpc, reminiscent of a molecular ring around an active galactic nucleus. Conversely, Q0957+561 is a clear case where CO is arising from the quasar host galaxy and one could notice as well that, in this case, no thermal dust emission is detected (dust in the host galaxy being at too low a temperature) and that only the CO J=2-1 transition is detected (cool and low density gas).

Therefore, various configurations seem to be found among the CO-detected high redshift sources. Thermal dust emission in the millimeter/submillimeter domain is a useful signature for assessing the origin of the CO-emitting gas. The mass of molecular gas remains large in these systems, even after correcting for the lens amplification, and is a factor 10 larger than in the case of gas-rich L* (Schechter 1976) galaxies (Sakamoto et al. 1999). If confirmed on a larger sample of quasars, this property might bring us some clues about quasar formation and the ignition of nuclear activity.

Acknowledgements. It is a pleasure to thank Roberto Neri for numerous interactions and helpful discussions. We wish to thank an anonymous referee for useful suggestions. DA, JPK and SG acknowledge support from CNRS. DA is gratefully indebted to travel support from CEA, ESO and IRAM.

References

Andreani, P., Cimatti, A., Loinard, L., & Röttgering, H. 2000, A&A, 354, L1
Barvainis, R., Alloin, D., & Bremer, M. 2002, A&A, 385, 399
Barvainis, R. & Ivison, R. 2002, ApJ, 571, 712
Barvainis, R., Maloney, P., Antonucci, R., & Alloin, D. 1997, ApJ, 484, 695
Bayet, E., Gerin, M., Phillips, T. G., & Contursi, A. 2004, A&A, 427, 45
Bertin, E. & Arnouts, S. 1996, A&AS, 117, 393
Carilli, C. L., Solomon, P., Vanden Bout, P., et al. 2005, ApJ, 618, 586
Fan, X., Strauss, M. A., Schneider, D. P., et al. 2003, AJ, 125, 1649
Frayer, D. T., Ivison, R. J., Scoville, N. Z., et al. 1998, ApJ, 506, L7
Greve, T. R., Bertoldi, F., Smail, I., et al. 2005, MNRAS, 359, 1165
Hainline, L. J., Scoville, N. Z., Yun, M. S., et al. 2004, ApJ, 609, 61
Kneib, J.-P., Alloin, D., Mellier, Y., et al. 1998, A&A, 329, 827
Kneib, J.-P., Ellis, R. S., Smail, I., Couch, W. J., & Sharples, R. M. 1996, ApJ, 471, 643
Krips, M., Neri, R., Eckart, A., et al. 2005, A&A, 431, 879
Lawrence, C. R., Bennett, C. L., Hewitt, J. N., et al. 1986, ApJS, 61, 105
Lehar, J., Burke, B. F., Conner, S. R., et al. 1997, AJ, 114, 48
Narayan, R. & Wallington, S. 1993, in Liege International Astrophysical Colloquia, ed. J. Surdej, D. Fraipont-Caro, E. Gosset, S. Refsdal, & M. Remy, p. 217
Sakamoto, K., Okumura, S. K., Ishizuki, S., & Scoville, N. Z. 1999, ApJ, 525, 691
Schechter, P. 1976, ApJ, 203, 297
Scoville, N. Z., Yun, M. S., Brown, R. L., & Vanden Bout, P. A. 1995, ApJ, 449, L109
Solomon, P. M., Downes, D., & Radford, S. J. E. 1992, ApJ, 398, L29
Solomon, P. M., Downes, D., Radford, S. J. E., & Barrett, J. W. 1997, ApJ, 478, 144
Tonry, J. L. & Kochanek, C. S. 1999, AJ, 117, 2034
Venturini, S. & Solomon, P. M. 2003, ApJ, 590, 740
Walter, F., Bertoldi, F., Carilli, C., et al. 2003, Nature, 424, 406
Weiß, A., Downes, D., Walter, F., & Henkel, C. 2005a, A&A, 440, L45
Weiß, A., Henkel, C., Downes, D., & Walter, F. 2003, A&A, 409, L41
Weiß, A., Walter, F., & Scoville, N. Z. 2005b, A&A, 438, 533
Wiklind, T. & Alloin, D. 2002, in LNP Vol. 608: Gravitational Lensing: An Astrophysical Tool, ed. F. Courbin & D. Minniti, p. 124